JOURNAL OF CATALYSIS **168,** 133–142 (1997)
ARTICLE NO. CA971629

Kinetic Implications of Dynamical Changes in Catalyst Morphology during Methanol Synthesis over Cu/ZnO Catalysts

C. V. Ovesen,* B. S. Clausen,* J. Schiøtz,† P. Stoltze,† H. Topsøe,* and J. K. Nørskov†

*Haldor Topsøe Research Laboratories, Nymøllevej 55, DK-2800 Lyngby, Denmark; and †Center for Atomic-scale Materials Physics, Department of Physics, The Technical University of Denmark, Building 307, DK-2800 Lyngby, Denmark

Received September 4, 1996; revised January 14, 1997; accepted January 14, 1997

In this paper a dynamic microkinetic model of the methanol synthesis reaction over Cu/ZnO catalysts is described. The model is based on surface science measurements and it includes the dynamic changes in particle shape and active surface area which have recently been observed by *in situ* EXAFS measurements to take place upon change in the redox potential of the reaction gas. It is suggested that the change in particle morphology is related to a change in the number of oxygen vacancies at the Zn–O–Cu interface. Furthermore, the structure sensitivity of the methanol synthesis reaction is also taken into account. The dynamic microkinetic model is seen to give a much better description of the kinetic measurements over a working methanol catalyst compared to a static microkinetic model. The new model also gives an explanation of the kinetic behavior during transient conditions. The dynamic aspects are seen to provide a basis for understanding the apparently conflicting reaction orders reported in the literature.

1. INTRODUCTION

In order to understand the performance and the mechanism of catalytic reactions, kinetic modeling has always played a central role (1–4). In the past it has been helpful to introduce simplified models based on assumptions regarding the nature of the rate-determining steps and most abundant surface intermediates. Recently, detailed surface insight has become available and this has allowed the introduction of more complete microkinetic treatments based on a fundamental understanding of the energetics of the individual steps (3–8). Irrespective of the kinetic approach used, it is typically assumed that the total concentration of active sites during different reaction conditions stays constant and that the main changes occurring are related to changes in the fraction of sites which are covered by reactants, intermediates, or products. However, it is not expected that the above assumptions may always be appropriate. In fact, many catalyst and surface science studies have shown that phenomena, such as spreading, surface reconstructions, or surface enrichment/segregation (in the case of alloy catalysts), may take place upon changing the gaseous environment (see, e.g., (9–17)). Nevertheless, quantitative information about such phenomena has been scarce and the consequences of the structural transformation have so far not been included in microkinetic models for catalytic reactions.

Recently, it has been shown that EXAFS and combined XRD/EXAFS (18–20) may provide interesting new possibilities for obtaining *in situ* structural insight and for following dynamical changes occurring during catalysis. In one such study the morphology of a methanol synthesis catalyst of Cu supported on ZnO was examined under different synthesis conditions. The EXAFS spectra showed reversible changes in the apparent coordination number for the Cu atoms when the oxidation potential of the gas was changed. Specifically, it was observed that a significant increase in the coordination number for Cu occurred when the catalyst was exposed to the most oxidizing gas. Changing back to the gas with the lower oxidation potential, the coordination number decreased again.

The results were interpreted as a change in the particle shape due to wetting/nonwetting phenomena induced by changes of the reduction potential of the gas phase. A change in reduction potential of the gas may change the composition at the Cu/ZnO interface, for example, by creation of oxygen vacancies in the reducing atmosphere or by changing the properties of the Schottky barrier between Cu and ZnO (21). This changes the free energy of the interface between the Cu particle and the support and it induces the change in particle morphology. The interpretation was supported by the fact that the phenomenon was not observed for Cu supported on SiO_2. A simple model was proposed based on calculations of the relative surface and interface energies of a particle (19) using the so-called Wulff construction (22). The dynamic behavior of the Cu/ZnO system has recently also been observed in another study (23).

In the present paper it will be shown how such insight can be used to formulate a "dynamic" microkinetic model for the methanol synthesis reaction over Cu/ZnO catalysts. It will be shown that this model can explain observations not accounted for in a recently developed "static" microkinetic

0021-9517/97 $25.00

model (24) as well as in transient experiments (25). The dynamic microkinetic model is also seen to provide a basis for understanding the apparently conflicting reaction orders reported in the literature.

2. RESULTS AND DISCUSSION

2.1. Microkinetic Analysis

In this section the kinetic consequences of the morphological changes will be discussed. First a description of the static microkinetic model will be given and then this model is extended to account for the dynamic morphological changes.

2.1.1. Static Microkinetic Model

A static microkinetic model of methanol synthesis reaction over Cu-based catalysts has recently been presented (24). It is based on 13 elementary reaction steps which all have been deduced from model studies on Cu single crystals.

$$H_2O(g) + * \rightleftarrows H_2O* \quad [1]$$

$$H_2O* + * \rightleftarrows OH* + H* \quad [2]$$

$$2OH* \rightleftarrows H_2O* + O* \quad [3]$$

$$OH* + * \rightleftarrows O* + H* \quad [4]$$

$$2H* \rightleftarrows H_2(g) + 2* \quad [5]$$

$$CO(g) + * \rightleftarrows CO* \quad [6]$$

$$CO* + O* \rightleftarrows CO_2* + * \quad [7]$$

$$CO_2* \rightleftarrows CO_2(g) + * \quad [8]$$

$$CO_2* + H* \rightleftarrows HCOO* + * \quad [9]$$

$$HCOO* + H* \rightleftarrows H_2COO* + * \quad [10]$$

$$H_2COO* + H* \rightleftarrows H_3CO* + O* \quad [11]$$

$$H_3CO* + H* \rightleftarrows CH_3OH* + * \quad [12]$$

$$CH_3OH* \rightleftarrows CH_3OH(g) + *, \quad [13]$$

where $*$ represents an empty site and $X*$ represents an adsorbed specie. The first 8 steps represent the elementary steps of the redox mechanism of the shift reaction, whereas the last 5 steps represent the synthesis of methanol through a formate intermediate. In this mechanism, methanol is synthesized from CO_2 in accordance with isotope labeling experiments (26, 27).

The kinetic model based on this reaction scheme is formulated assuming that all reactions are in equilibrium except for reaction steps [2], [4], [7], and [11]. Reaction steps [2], [4], and [7] are all steps which may be slow during the shift reaction (28, 29), whereas reaction step [11] represents the slow step for methanol synthesis (24). Based on the above, the following set of rate and equilibrium equations can be written:

$$K_1 \frac{P_{H_2O}}{P_0}\theta_* = \theta_{H_2O*} \quad [14]$$

$$r_2 = k_2\theta_{H_2O*}\theta_* - \frac{k_2}{K_2}\theta_{OH*}\theta_{H*} \quad [15]$$

$$K_3\theta_{OH*}^2 = \theta_{H_2O*}\theta_{O*} \quad [16]$$

$$r_4 = k_4\theta_{OH*}\theta_* - \frac{k_4}{K_4}\theta_{O*}\theta_{H*} \quad [17]$$

$$K_5\theta_{H*}^2 = \frac{P_{H_2}}{P_0}\theta_*^2 \quad [18]$$

$$K_6 \frac{P_{CO}}{P_0}\theta_* = \theta_{CO*} \quad [19]$$

$$r_7 = k_7\theta_{CO*}\theta_{O*} - \frac{k_7}{K_7}\theta_{CO_2*}\theta_* \quad [20]$$

$$K_8\theta_{CO_2*} = \frac{P_{CO_2}}{P_0}\theta_* \quad [21]$$

$$K_9\theta_{H*}\theta_{CO_2*} = \theta_{HCOO*}\theta_* \quad [22]$$

$$K_{10}\theta_{HCOO*}\theta_{H*} = \theta_{H_2COO*}\theta_* \quad [23]$$

$$r_{11} = k_{11}\theta_{H_2COO*}\theta_{H*} - \frac{k_{11}}{K_{11}}\theta_{H_3CO*}\theta_* \quad [24]$$

$$K_{12}\theta_{H_3CO*}\theta_{H*} = \theta_{CH_3OH*}\theta_* \quad [25]$$

$$K_{13}\theta_{CH_3OH*} = \frac{P_{CH_3OH}}{P_0}\theta_* \quad [26]$$

K_i is the equilibrium constant for reaction step i, whereas k_i is the rate constant for reaction step i. P_i is the partial pressure of specie i, whereas P_0 is the reference pressure chosen to be 1 atm. This implies that the equilibrium constant for an adsorption reaction is dimensionless and that the rate constant has the unit molecules per site per second.

The model calculations presented in Ref. (24) were based on the assumption that the number of active sites is constant. The rate constant for methanol synthesis was deduced from studies over the Cu(100) plane (30). All the other low index planes were assumed to have the same activities. Recently, the rate of methanol synthesis over the two other low index surface planes has also been measured (31, 32). Thus, it has been possible in the present analysis also to take into account the structure sensitivity of this reaction. The observed rate of methanol synthesis r_{obs} over a catalyst will then be an average of the rates over the exposed facets and can thus be expressed as

$$r_{obs} = (\eta r_{100} + \varepsilon r_{110} + (1 - \eta - \varepsilon) r_{111})N, \quad [27]$$

where η is the ratio of the number of sites on the (100) plane relative to the total number of sites N, ε is the ratio of

the number of sites on the (110) plane relative to the total number of sites, and r_i is the specific rate over a surface site in plane *i*. The contribution to the rate from corner and edge sites is neglected presently. This may be reasonable since the copper particles for the catalysts studied in the present work are greater than 20 Å.

The analytic expressions for the rate over the three surface planes are the same but the value of the equilibrium and rate constants are different. An analytic expression for the rate of methanol synthesis can be derived from Eqs. [14]–[26] but is not shown here since it is very space consuming. The contribution to the overall rate from one surface plane is a combination of how fast the reaction is over this plane and how much of the specific surface plane is present during reaction.

2.1.1.1. Model parameters for Cu(100). In the model the rate constants are described by the Arrhenius equation and the equilibrium constants are calculated from the partition function of the intermediates. A detailed description of this procedure has been given in (24). The partition function of a specific molecule is calculated from the vibrational frequencies and the ground state energy of the molecule. For a gas-phase molecule, this information can be found in the JANAF Tables (33), whereas for an adsorbed molecule the vibrational frequencies are typically taken from available HREELS spectra. The ground state energy for gaseous molecules is determined from the standard enthalpy of formation, whereas the ground state energy for adsorbed molecules is determined from TPD spectra. When analyzing a TPD spectrum the desorption rate constant is expressed by the forward rate constant and the equilibrium constant using the principle of microscopic reversibility. The forward rate constant is typically measured from adsorption studies or can be estimated form transition state theory. The ground state energy of the adsorbed state is then estimated from the TPD spectrum for optimal agreement between the model and the TPD spectrum. This procedure assures a consistent treatment of the adsorption desorption process in agreement with the principle of microscopic reversibility. The accuracy of the ground state energy determined by this method is typically 3 kJ/mole.

The rate constant for methanol synthesis, where reaction step [11] was assumed rate limiting, was deduced from synthesis experiments over a Cu(100) single crystal in a $CO_2 + H_2$ gas mixture with a $CO_2 : H_2$ ratio of 1 at a total pressure of 2 bar and temperatures ranging from 483 to 563 K (30). Both vibrational frequencies, ground state energies, and rate constants for reaction [1] to [13] for the Cu(100) plane were reported in Ref. (24) and are shown in Tables 1 and 2.

2.1.1.2. Model parameters for Cu(110). In the evaluation of the parameters for the Cu(110) plane, the parameters for the Cu(100) plane are used as a starting point. The parameters that are most important for methanol synthesis conditions are then reinterpreted using data obtained for the Cu(110) plane. This is essentially the equilibrium constant for CO adsorption, the equilibrium constant for formate decomposition, and the rate constant for methanol synthesis. From CO TPD studies of Cu single crystals it is found that the desorption is structure sensitive. The CO desorption peak maximum for Cu(110) occurs at a temperature approximately 40 K higher than for Cu(100) (34, 35). Similarly, the formate decomposition peak maximum over Cu(110) occurs at a temperature approximately 40 K higher than on Cu(100) (36, 37). If it is assumed that the synthesis rate of formate over Cu(110) is the same as over Cu(100), formate is found to be 8 kJ/mole more stable on Cu(110) than on Cu(100). The thermodynamic parameters are listed in Table 1.

The activity of methanol synthesis has recently been measured over Cu(110) in a $CO_2 + H_2$ gas mixture with a $CO_2 : H_2$ ratio of 0.09 at a total pressure of 5.1 bar and temperatures ranging from 490 to 530 K [32]. Using the microkinetic model consisting of reactions [1]–[13] and the thermodynamic parameters for the Cu(110) plane given in Table 1, it is possible to estimate the rate constant for the rate-limiting step [11] in the mechanism. The agreement between model and experiment obtained from this estimate is shown in Fig. 1. The activation energy for the rate-limiting step Cu(110) is the same as over Cu(100), while the preexponential factor is 25 times higher.

2.1.1.3. Model parameters for Cu(111). For the Cu(111) plane, the same parameters as for the Cu(100) plane are used except for the rate constant for methanol synthesis. Although no detailed study of methanol synthesis over Cu(111) has yet appeared, the activity at 523 K in a $CO_2 + H_2$ gas mixture with a $CO_2 : H_2$ ratio of 0.33 and a total pressure of 18 bar was recently reported (31). Using the thermodynamic parameters determined for the Cu(111) plane and fitting the rate constant of reaction step [11] from these measurements indicates that the rate constant over

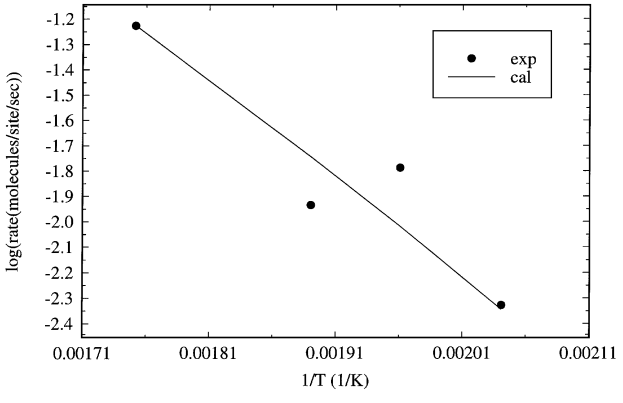

FIG. 1. Rate of methanol synthesis over Cu(110) at 4.67 bar H_2 and 0.41 bar CO_2. Solid circles, measured rate, adapted from Ref. (32). Solid line calculated from static microkinetic model.

TABLE 1

Thermodynamic Parameters Used in the Model

Species	Vibrational parameters	Energy E_g
$H_2(g)$	$B = 60.9\ cm^{-1}$, $\sigma = 2$, $\nu_1 = 4405\ cm^{-1}$	−35.0 kJ/mol
H∗	$\nu_\perp = 1121\ cm^{-1}$, $\nu_\parallel = 928(2)\ cm^{-1}$	Cu(100): −40.7 kJ/mol Cu(110): −40.7 kJ/mol Cu(111): −40.7 kJ/mol
$H_2O(g)$	$I_A I_B I_C = 5.77 \times 10^{-141}\ kg^3\ m^6$, $\sigma = 2$, $\nu_1 = 1595\ cm^{-1}$, $\nu_2 = 3657\ cm^{-1}$, $\nu_3 = 3755\ cm^{-1}$	−305.6 kJ/mol
H_2O∗	$\nu_\perp = 460\ cm^{-1}$, $\nu_\parallel = 48(2)\ cm^{-1}$, $\nu_r = 745(3)\ cm^{-1}$, $\nu_1 = 1600\ cm^{-1}$, $\nu_2 = 3370(2)\ cm^{-1}$	Cu(100): −362.6 kJ/mol Cu(110): −366.0 kJ/mol Cu(111): −362.6 kJ/mol
O∗	$\nu_\perp = 391\ cm^{-1}$, $\nu_\parallel = 508(2)\ cm^{-1}$	−243.8 kJ/mol
OH∗	$\nu_\perp = 280\ cm^{-1}$, $\nu_\parallel = 49(2)\ cm^{-1}$, $\nu_r = 670(2)\ cm^{-1}$, $\nu_\perp = 3380\ cm^{-1}$	Cu(100): −309.6 kJ/mol Cu(110); −309.6 kJ/mol Cu(111): −309.6 kJ/mol
$CO(g)$	$B = 1.93\ cm^{-1}$, $\sigma = 1$, $\nu_1 = 2170\ cm^{-1}$	−132.2 kJ/mol
CO∗	$\nu_\perp = 343\ cm^{-1}$, $\nu_\parallel = 24(2)\ cm^{-1}$, $\nu_r = 290(3)\ cm^{-1}$, $\nu_1 = 2089\ cm^{-1}$	Cu(100): −186.1 kJ/mol Cu(110): −199.3 kJ/mol Cu(111): −186.1 kJ/mol
$CO_2(g)$	$B = 0.39\ cm^{-1}$, $\sigma = 2$, $\nu_1 = 667\ cm^{-1}$, $\nu_2 = 1343\ cm^{-1}$, $\nu_3 = 2350\ cm^{-1}$	−433.0 kJ/mol
CO_2∗	$\nu_\perp = 410\ cm^{-1}$, $\nu_\parallel = 31(2)\ cm^{-1}$, $\nu_r = 13(2)\ cm^{-1}$, $\nu_1 = 667\ cm^{-1}$, $\nu_2 = 1343\ cm^{-1}$, $\nu_3 = 2349\ cm^{-1}$	Cu(100): −460.3 kJ/mol Cu(110): −459.8 kJ/mol Cu(111): −460.3 kJ/mol
HCOO∗	$\nu_\perp = 322\ cm^{-1}$, $\nu_\parallel = 36(2)\ cm^{-1}$, $\nu_r = 400(3)\ cm^{-1}$, $\nu_1 = 758\ cm^{-1}$, $\nu_2 = 1331\ cm^{-1}$, $\nu_3 = 1640\ cm^{-1}$, $\nu_4 = 2879\ cm^{-1}$, $\nu_5 = 1073\ cm^{-1}$, $\nu_6 = 1377\ cm^{-1}$	Cu(100): −552.7 kJ/mol Cu(110): −560.7 kJ/mol Cu(111): −552.7 kJ/mol
CH_3O∗	$\nu_\perp = 400\ cm^{-1}$, $\nu_\parallel = 37(2)\ cm^{-1}$, $\nu_r = 360(3)\ cm^{-1}$, $\nu_1 = 1020\ cm^{-1}$, $\nu_2 = 1150(2)\ cm^{-1}$, $\nu_3 = 1460(3)\ cm^{-1}$, $\nu_4 = 2840\ cm^{-1}$, $\nu_5 = 2940(2)\ cm^{-1}$	Cu(100): −300.0 kJ/mol Cu(110): −300.0 kJ/mol Cu(111): −300.0 kJ/mol
H_2COO∗	$\nu_\perp = 405\ cm^{-1}$, $\nu_\parallel = 30(2)\ cm^{-1}$, $\nu_r = 400(3)\ cm^{-1}$, $\nu_1 = 630\ cm^{-1}$, $\nu_2 = 960\ cm^{-1}$, $\nu_3 = 1090\ cm^{-1}$, $\nu_4 = 1220(2)\ cm^{-1}$, $\nu_5 = 1420\ cm^{-1}$, $\nu_6 = 1480\ cm^{-1}$, $\nu_7 = 2920\ cm^{-1}$, $\nu_8 = 3000\ cm^{-1}$	Cu(100): −568.0 kJ/mol Cu(110): −568.0 kJ/mol Cu(111): −568.0 kJ/mol
$CH_3OH(g)$	$I_A = 6.68 \times 10^{-47}\ kg\ m^2$, $I_B = 34.00 \times 10^{-47}\ kg\ m^2$, $I_C = 35.31 \times 10^{-47}\ kg\ m^2$, $\sigma = 3$, $\nu_1 = 270\ cm^{-1}$, $\nu_2 = 1033\ cm^{-1}$, $\nu_3 = 1060\ cm^{-1}$, $\nu_4 = 1165\ cm^{-1}$, $\nu_5 = 1345\ cm^{-1}$, $\nu_6 = 1477(2)\ cm^{-1}$, $\nu_7 = 1455\ cm^{-1}$, $\nu_8 = 2844\ cm^{-1}$, $\nu_9 = 2960\ cm^{-1}$, $\nu_{10} = 3000\ cm^{-1}$, $\nu_{11} = 3681\ cm^{-1}$	−342.8 kJ/mol
CH_3OH∗	$\nu_\perp = 290\ cm^{-1}$, $\nu_\parallel = 36(2)\ cm^{-1}$, $\nu_r = 360(3)\ cm^{-1}$, $\nu_1 = 750\ cm^{-1}$, $\nu_2 = 820\ cm^{-1}$, $\nu_3 = 1030\ cm^{-1}$, $\nu_4 = 1150(2)\ cm^{-1}$, $\nu_5 = 1470(3)\ cm^{-1}$, $\nu_6 = 2860\ cm^{-1}$, $\nu_7 = 2970(2)\ cm^{-1}$, $\nu_8 = 3320\ cm^{-1}$	Cu(100): −413.3 kJ/mol Cu(110): −413.3 kJ/mol Cu(111): −413.3 kJ/mol

Note. B, I_A, and σ are the rotational constants, the moment of inertia, and the symmetry number of the gas-phase molecule, respectively. Vibrational modes are denoted by ν_j and the degeneracy of a frequency is enclosed in parentheses. The frequency $\nu_\perp$, $\nu_\parallel$, and ν_r are the frustrated translational orthogonal frequency, the frustrated translational parallel frequency, and the frustrated rotational frequency, respectively.

this plane is approximately five times lower than the rate constant over Cu(100). The rate constants used in the model are shown in Table 2.

2.1.2. Dynamic Microkinetic Model

In order to develop a microkinetic model which can account for the observed changes in the surface area ("dynamic microkinetic model"), it is necessary to incorporate a description of the change in the number of active sites as a function of changes in the reaction conditions.

As mentioned in the Introduction, the observed change in particle morphology is presumably caused by a change in the contact surface free energy between the Cu particle and the support. Such a change in the surface free energy is likely if the concentration of oxygen vacancies at the Zn−O−Cu interface varies with change in the reduction potential of the gas phase. The model used to explain the observed change in particle morphology was based on calculations of the relative surface and interface free energies of a particle applying the so called Wulff construction (19).

TABLE 2

Rate Constants Used in the Kinetic Model

Cu(100)		
k_2	$A_2 = 2.6 \times 10^{14}\ s^{-1}$	$E_2 = 114.0$ kJ/mol
k_4	$A_4 = 2.3 \times 10^{8}\ s^{-1}$	$E_4 = 99.1$ kJ/mol
k_7	$A_7 = 1.8 \times 10^{13}\ s^{-1}$	$E_7 = 86.9$ kJ/mol
k_9	$A_9 = 2.1 \times 10^{10}\ s^{-1}$	$E_9 = 78.0$ kJ/mol
k_{11}	$A_{11} = 7.8 \times 10^{20}\ s^{-1}$	$E_{11} = 161.8$ kJ/mol
Cu(110)		
k_2	$A_2 = 7.7 \times 10^{12}\ s^{-1}$	$E_2 = 90.8$ kJ/mol
k_4	$A_4 = 6.3 \times 10^{8}\ s^{-1}$	$E_4 = 114.2$ kJ/mol
k_7	$A_7 = 1.8 \times 10^{13}\ s^{-1}$	$E_7 = 85.4$ kJ/mol
k_9	$A_9 = 2.1 \times 10^{10}\ s^{-1}$	$E_9 = 78.0$ kJ/mol
k_{11}	$A_{11} = 2.0 \times 10^{22}\ s^{-1}$	$E_{11} = 161.8$ kJ/mol
Cu(111)		
k_2	$A_2 = 2.6 \times 10^{14}\ s^{-1}$	$E_2 = 114.0$ kJ/mol
k_4	$A_4 = 2.3 \times 10^{8}\ s^{-1}$	$E_4 = 99.1$ kJ/mol
k_7	$A_7 = 1.1 \times 10^{13}\ s^{-1}$	$E_7 = 72.2$ kJ/mol
k_9	$A_9 = 2.1 \times 10^{10}\ s^{-1}$	$E_9 = 78.0$ kJ/mol
k_{11}	$A_{11} = 1.6 \times 10^{20}\ s^{-1}$	$E_{11} = 161.8$ kJ/mol

In the Wulff construction, the shape of a free particle of a given volume is simply determined by the condition that the total free energy of the surfaces is at minimum. To describe a particle in contact with a substrate, the free energy of the interface is replaced with a "contact-surface free energy," γ. This contact-surface free energy is the difference between the interface energy $\gamma_{\text{interface}}$ and the surface energy of the substrate $\gamma_{\text{substrate}}$, i.e., $\gamma = \gamma_{\text{interface}} - \gamma_{\text{substrate}}$. It is described relative to the free energy of a similar free surface γ_0 by the parameter γ/γ_0. This means that if γ/γ_0 is 1 the shape of the original free particle is obtained, whereas if γ/γ_0 is -1 the particle degenerates to a two-dimensional surface where Cu is epitaxially grown on Zn.

Figure 2 shows the surface area of the different facets of the particle with the (100) plane, the (110) plane, and the (111) plane, respectively, attached to the substrate at different values of γ/γ_0 calculated from the Wulff construction. For positive values of γ/γ_0 it is seen that the (111) facet is the dominating facet, whereas for large negative values of γ/γ_0, the facet attached to the substrate dominates.

It appears reasonable to assume that under methanol/shift conditions, the concentration of the oxygen vacancies in the ZnO is predominantly determined by the following equilibrium reactions:

$$H_2(g) + \text{Zn–O} \rightleftarrows H_2O(g) + \text{Zn–}\square \qquad [28]$$

$$CO(g) + \text{Zn–O} \rightleftarrows CO_2(g) + \text{Zn–}\square, \qquad [29]$$

where $\square$ is an oxygen vacancy in the ZnO.

At the Zn–O–Cu interface, the concentration of oxygen vacancies is similarly assumed to be determined by the two equations

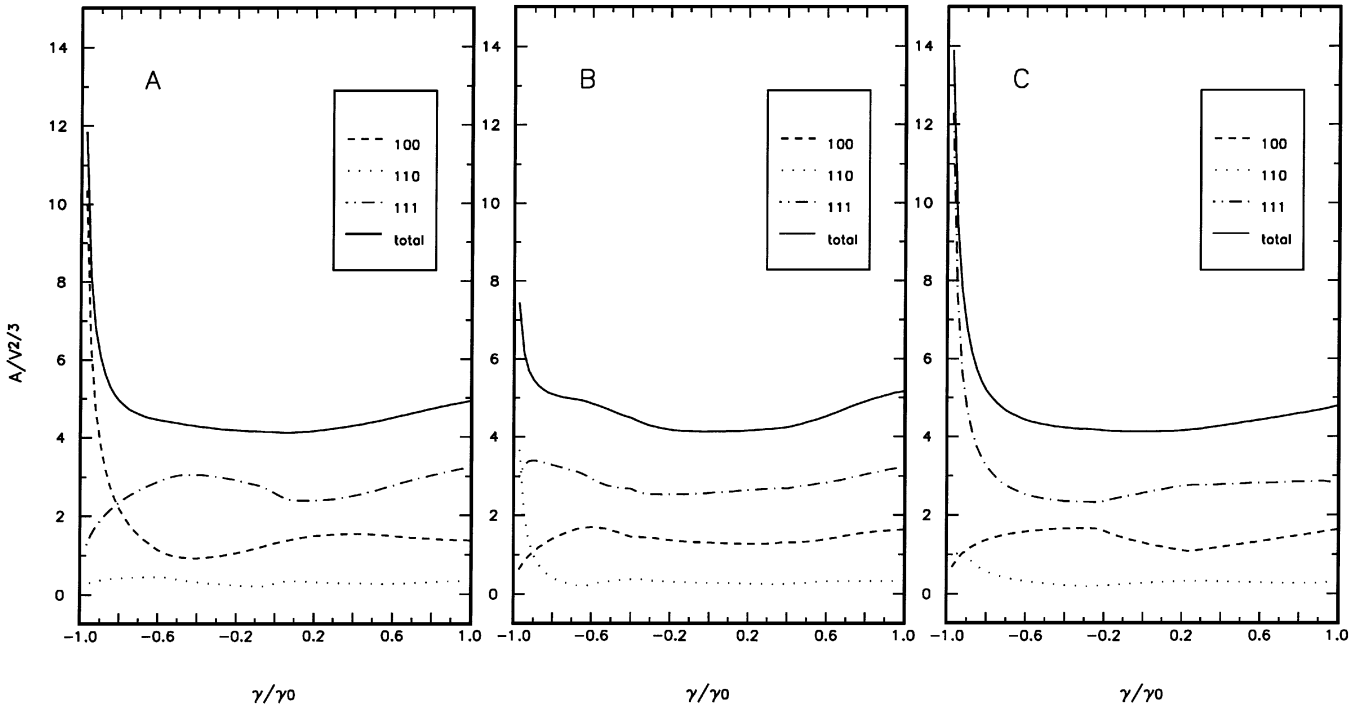

FIG. 2. The dimensionless surface area $A/V^{2/3}$ of the different facets as well as the total area versus the contact surface free energy γ/γ_0. (A) Calculated from the Wulff construction assuming that one of the (100) plane of the particle is attached to the substrate. (B) Calculated from the Wulff construction assuming that one of the (110) plane of the particle is attached to the substrate. (C) Calculated from the Wulff construction assuming that one of the (111) plane of the particle is attached to the substrate.

$$H_2(g) + Zn{-}O{-}Cu \rightleftarrows H_2O(g) + Zn{-}\square{-}Cu \quad [30]$$

$$CO(g) + Zn{-}O{-}Cu \rightleftarrows CO_2(g) + Zn{-}\square{-}Cu. \quad [31]$$

Equations [30] and [31] give the following three equations:

$$K_1 = \frac{P_{H_2O}}{P_{H_2}} \cdot \frac{[Zn{-}\square{-}Cu]}{[Zn{-}O{-}Cu]} \quad [32]$$

$$K_2 = \frac{P_{CO_2}}{P_{CO}} \cdot \frac{[Zn{-}\square{-}Cu]}{[Zn{-}O{-}Cu]} \quad [33]$$

$$[Zn{-}O{-}Cu] = 1 - [Zn{-}\square{-}Cu], \quad [34]$$

where $[X]$ is the interface concentration of species X.

These equations describe the dependence of the oxygen vacancies at the interface by the gas-phase reduction potential. In order to relate the reduction potential to the relative surface contact free energy γ/γ_0, a description of the relation between the concentration of oxygen vacancies and the surface contact free energy is needed. For simplicity, we assume the relation to be linear:

$$[Zn{-}\square{-}Cu] = (1 - \gamma/\gamma_0)/2. \quad [35]$$

The limit where γ/γ_0 is 1 corresponds to a free Cu particle with no oxygen vacancies, whereas the other limit where γ/γ_0 is -1 corresponds to epitaxial growth of Cu on Zn and a full monolayer of oxygen vacancies in the interface.

From Eqs. [32] through [35], it is now possible to make a relation between reduction potential and the relative surface contact free energy:

$$\gamma/\gamma_0 = \frac{1 - \sqrt{K_1K_2\frac{P_{H_2}P_{CO}}{P_{H_2O}P_{CO_2}}}}{1 + \sqrt{K_1K_2\frac{P_{H_2}P_{CO}}{P_{H_2O}P_{CO_2}}}}, \quad [36]$$

where K_1K_2, expressed as a function of the free energy of reactions [30] and [31] is given by

$$K_1K_2 = \exp\left(-\frac{\Delta G}{RT}\right) \quad [37]$$

Thus, if ΔG is known it is possible to calculate the surface contact free energy and thus to calculate the surface area (i.e., the number of active sites) from the Wulff construction shown in Fig. 2. The change in Gibbs free energy for creation of oxygen vacancies at the Zn–O–Cu interface has to the best of our knowledge not been determined and therefore it must be estimated. This has been done by choosing the synthesis gas composition as reference point and then estimate ΔG for a fixed value of the surface contact free energy γ/γ_0, which is called $(\gamma/\gamma_0)_{FIX}$. ΔG is then given by

$$\Delta G = -RT \cdot \ln\left(\left(\frac{1 - (\gamma/\gamma_0)_{FIX}}{1 + (\gamma/\gamma_0)_{FIX}}\right)^2 \Big/ \frac{P_{H_2}P_{CO}}{P_{H_2O}P_{CO_2}}\right). \quad [38]$$

The number of active sites N on the catalyst is

$$N = N_0 \frac{\sum_i f_i(\gamma/\gamma_0)D_i}{\sum_j f_j((\gamma/\gamma_0)_{FIX})D_j}, \quad [39]$$

where $f_i\,(\gamma/\gamma_0)$ is the value of the surface area taken from Fig. 2 for surface plane i, D_i is the site density of this plane, and N_0 is a constant factor expressing the number of sites of the actual catalyst at fixed conditions. This means that η, the ratio of the number of sites on the 100 plane relative to the total number of sites, used in Eq. [27] expressed as a function of f is given by

$$\eta = \frac{f_{100}(\gamma/\gamma_0)D_{100}}{\sum_j f_j(\gamma/\gamma_0)D_j}. \quad [40]$$

A similar expression can be evaluated for ε.

2.2. Test of Dynamic Model

Graff *et al.* (38, 39) have measured the rate of methanol synthesis over a commercial $Cu/ZnO/Al_2O_3$ catalyst in a continuous stirred tank reactor. In these experiments, the total pressure was varied from 15 to 50 atm and the temperature from 484 to 517 K.

First these data are analyzed assuming a constant surface area, i.e., constant number of active sites with a distribution of surface planes as determined from the Wulff construction of a free particle, i.e., $\gamma/\gamma_0 = 1$. The agreement between model and experiments is shown in Fig. 3A. Graff *et al.* (32, 39) have not estimated the error on the measured rate of methanol synthesis. Generally the error on such measurements are 10% (29). It is seen that the static microkinetic model reproduces the magnitude of the rate and the trends quite well. Nevertheless, upon closer examination it is evident that the data can be grouped into two families depending on the inlet gas compositions, i.e., the reduction potential of the gas phase. A sensitivity analysis of the model parameters showed that the model and the experiments cannot be brought in agreement unless the parameters are severely changed and thus would bring them in disagreement with the surface chemistry of the reaction, i.e., TPD experiments. In the literature there has been suggestion that the first hydrogenation of formate, i.e., reaction step [10] is rate limiting under methanol synthesis conditions (44). We have also examined this proposal but assuming this reaction step to be rate limiting cannot bring the experiments and the model in agreement.

In order to introduce the dynamic aspects, it is assumed that the particle changes its shape as described above (see Section, 2.1.2). The effect of choosing different values of $(\gamma/\gamma_0)_{FIX}$ or equivalent values of ΔG is seen in Table 3. The free energy varies from -8 to 22 kJ/mol which is between the values for creation of oxygen vacancies in bulk CuO (-239 kJ/mol at 500 K (33)) and bulk ZnO (142 kJ/mol at

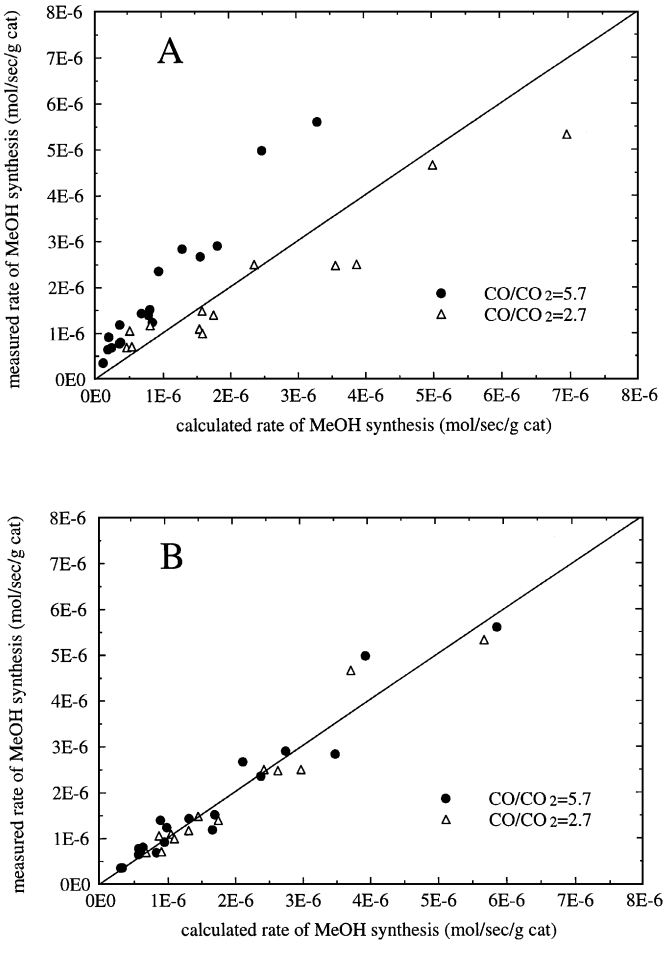

FIG. 3. Comparison of calculated rate with measured rate of methanol synthesis over a $Cu/ZnO/Al_2O_3$ catalyst. The calculated rate is obtained from the dynamic microkinetic model assuming the interface is (110). Inlet gas compositions: 12% CO, 2.1% CO_2, 85.9% H_2 (solid circle), 17.9% CO, 6.7% CO_2, 75.4% H_2 (open triangle). (A) A constant surface area is assumed. (B) A surface area dynamically dependent of the gaseous environment is assumed. Experimental data adapted from Refs. (38, 39).

500 K (33)) showing that the value of ΔG from a physical point of view is reasonable.

The difference between the calculated and the measured rate is minimized by varying N_0 of Eq. [39]. The agreement with the reaction data for different choice of $(\gamma/\gamma_0)_{FIX}$ is shown in Table 3 for particles attached with the (100), the (110), or the (111) facet against the substrate. In general, the best description of the experimental data is obtained when the surface area is allowed to depend dynamically on the gas-phase composition. Furthermore, the best agreement is obtained when there is a low contact surface free energy between the particle and the support. It is important to note that a one-parameter fit is used both in the case of a constant surface area (Fig. 3A) and in the case of a dynamic surface area (for each choice of $(\gamma/\gamma_0)_{FIX}$) (Fig. 3B).

The best agreement is obtained in the case where the Cu particle is attached with the (110) plane against the substrate. The result for $(\gamma/\gamma_0)_{FIX} = -0.90$ and $\Delta G = -2$ kJ/mol is shown in Fig. 3B. It is seen that the separation of reaction data into two groups is no longer present. Thus allowing the number of active sites to depend dynamically on the gaseous environment gives a better description of the kinetics. The reduction potential of the reaction data (38, 39) has a large variation which according to the model causes the surface area to change by 50% (Fig. 4). When going from the reaction data with inlet $CO/CO_2 = 2.7$ to the reaction data with inlet ratio $CO/CO_2 = 5.7$ the number of active sites increases due to an increase in the area of the (110) surface plane. This has a remarkable effect on the overall reaction rate since the methanol synthesis is structure sensitive and the rate is fastest over this surface plane. The calculated surface areas agree within a factor of two with the reported surface areas of similar catalysts measured by H_2 TPD (25) showing that reasonable values of the number of active sites are used in the model.

TABLE 3

Determination of the Free Energy ΔG for Creation of Oxygen Vacancies at the Zn–O–Cu Interface

$(\gamma/\gamma_0)_{FIX}$	ΔG (kJ/mol)	Sqsum (100) interface	Sqsum (110) interface	Sqsum (111) interface
0	22.2	2.41×10^{-11}	2.28×10^{-11}	2.70×10^{-11}
−0.25	18.0	1.61×10^{-11}	2.78×10^{-11}	2.58×10^{-11}
−0.50	13.2	1.42×10^{-11}	2.78×10^{-11}	2.09×10^{-11}
−0.75	6.2	1.43×10^{-11}	1.33×10^{-11}	1.28×10^{-11}
−0.85	1.6	1.45×10^{-11}	5.87×10^{-12}	1.32×10^{-11}
−0.90	−2.0	1.44×10^{-11}	4.09×10^{-12}	1.54×10^{-11}
−0.95	−7.8	2.21×10^{-11}	4.91×10^{-12}	1.91×10^{-11}

Note. The choice of fix point for catalyst exposed to synthesis gas and its consequence for the value of ΔG. For each choice, the best description of reaction data adapted from Refs. (35, 36) expressed as the square sum (sqsum) of the absolute difference between measured and calculated rate is shown. A static microkinetic model gives sqsum $= 2.95 \times 10^{-11}$.

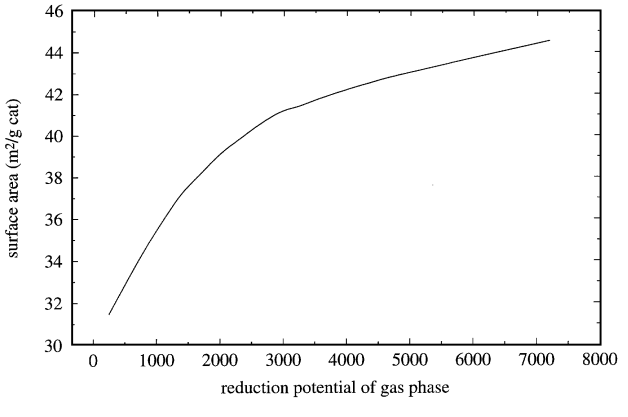

FIG. 4. The estimated surface area as a function of the reduction potential of the gas phase ($P_{CO}\ P_{H_2}/(P_{CO_2}\ P_{H_2O})$) for the reaction data shown in Fig. 3B.

The agreement for the present data assuming that either the (100) or the (111) plane is attached against the substrate is also good (Table 3). Thus, it is not possible based on these data to determine the growth mode for the Cu particle on the ZnO.

Studies of the chemisorption of formate on small Cu islands on ZnO(0001) showed properties much like the Cu(110) plane (40) which would suggest that in the actual catalyst the Cu particles are supported with the (110) facet against the substrate. Recent *in situ* FTIR studies of the shift in frequency of the CO adsorption band over a Cu/ZnO catalyst under different synthesis conditions may provide a link between these model studies and the actual catalyst (41).

It is clear that the dynamic microkinetic model gives an improved description of the present kinetic data. In the following, the model will be tested against other independent measurements.

Studies of methanol synthesis under transient conditions have been reported previously (25). In these experiments, a methanol catalyst was first exposed to a highly reducing gas mixture 6% CO in H_2 at 493 K and 1 atm total pressure (Fig. 5). In this gas mixture, essentially no methanol is produced since methanol is predominantly synthesized from CO_2. The inlet gas is then in one step switched to a gas containing 5% CO and 5% CO_2 in H_2. It is seen that the production of methanol increases almost instantaneously, goes through a maximum, and then decreases slowly to the steady-state value. The static microkinetic model, which assumes that the number of sites is constant, predicts that the production of methanol increases after the switch to the CO_2-containing gas and then converges to a steady-state value without going through a maximum. Thus, the observed maximum is not due to changes in coverages on the surface. The observed maximum can, however, be understood within the present dynamic microkinetic model. In the reducing gas, the surface area is high. When switching to the CO_2-containing gas, initially a high production of methanol is observed due to the high surface area obtained in the reducing gas. However, as the Cu particles equilibrate with the gas with the lower reduction potential, the surface area decreases causing a decrease in the methanol production rate.

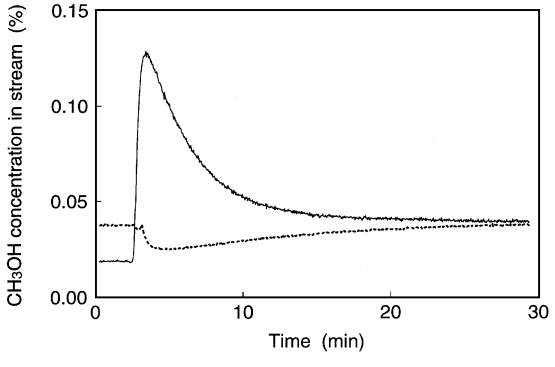

FIG. 5. Concentration of methanol in the plug flow reactor outlet in transient studies of methanol synthesis. Solid line, the feed gas composition was changed from about 6% CO in H_2 (34 ml/min (at STP)) in one step to about 5% CO_2, 5% CO, and balance H_2 (42 ml/min (at STP)) when the reactor was operating at 493 K and 1 atm total pressure. Dashed line: The feed gas composition was changed from about 6% CO_2 in H_2 (36 ml/min (at STP)) in one step to about 5% CO_2, 5% CO, and balance H_2 (42 ml/min (at STP)) when the reactor was operating at 473 K and 1 atm total pressure. Data adapted from Ref. (25).

If instead the catalyst initially is exposed to a less reducing gas (6% CO_2 in H_2 at 473 K and 1 atm total pressure) and then switched to a more reducing gas (5% CO, 5% CO_2 in H_2), a decrease in the methanol production rate is observed followed by a slow increase to the steady-state value (Fig. 5). The static microkinetic model predicts a decrease in the rate of methanol production after the switch to the CO-containing gas. Thus, the observed minimum is not due to changes in coverages on the surface. The observed minimum can, on the other hand, be understood within the present dynamic model using the same arguments as above.

Since in both cases the reaction is far from equilibrium for methanol synthesis and is studied at low pressure where the coverage is low, the observed conversion is proportional to the rate. This implies that the change in rate going from the 6% CO in H_2 gas to the synthesis gas is much higher than the decrease in rate observed going from the 6% CO_2 in H_2 to the synthesis gas. This is in good agreement with the results from the Wulff construction (Fig. 2) which predicts that a larger change in surface area is observed going from the left in Fig. 2 to the middle than when going from the right to the middle.

It is seen that the dynamic microkinetic model can describe several independent experiments that the static model was not able to describe. The result therefore suggests that the morphology changes that were observed with EXAFS do have very important kinetic implications under relevant methanol synthesis conditions. We are presently examining if there could be other physical phenomena contributing to the observed changes of methanol synthesis.

2.3. Consequence for Interpretation of Reaction Orders

It has previously been shown that a microkinetic model gives the possibility to evaluate and understand the origin of reaction orders (3, 4). The present dynamic microkinetic model gives the possibility to evaluate the consequence of dynamic behavior on the apparent reaction orders.

When estimating apparent reaction orders, it is assumed that the number of sites is constant. The reaction order, α_i, for component i is in this case simply defined by

$$\alpha_i = \frac{\delta \ln(r_+)}{\delta \ln(P_i)}, \qquad [41]$$

where r_+ is the forward rate.

The apparent reaction rate r_{app} is a product of the static reaction rate r_{static} times the relative change in surface area:

$$r_{app} = \frac{A_{dynamic}}{A_{constant}} r_{static}. \quad [42]$$

The apparent reaction order α_{app} will then be given by

$$\alpha_{app} = \frac{\delta \ln(r_{static})}{\delta \ln(P_i)} + \frac{P_i}{A_{dynamic}} \frac{\delta A_{dynamic}}{\delta P_i}, \quad [43]$$

where the first term is denoted the static reaction order α_s and the second term is denoted α_d which is the contribution to the reaction order arising from the dynamic change of the surface area. The term $\delta(A_{dynamic})/\delta(P_i)$ is proportional to the derivative of the curves shown in Fig. 2. Thus, in the regime where $\gamma/\gamma_0 < 0$, i.e., reducing conditions, the value of α_d is

$$\alpha_d < 0 \text{ for oxidizing gases}$$

$$\alpha_d > 0 \text{ for reducing gases,}$$

whereas when $\gamma/\gamma_0 > 0$, i.e., oxidizing conditions:

$$\alpha_d > 0 \text{ for oxidizing gases}$$

$$\alpha_d < 0 \text{ for reducing gases.}$$

For methanol synthesis conditions, the present analysis has shown that $\gamma/\gamma_0 < 0$. It is often reported in the literature that the apparent reaction order of water is negative under methanol synthesis conditions (42–45). However, the concentration of water is relatively low under these conditions (42) and from surface science studies, it is known that water adsorbs weakly on the surface (24). Thus, the apparent negative reaction order for water is probably not due to blocking of sites by water. The present findings suggest that it is caused by a decrease in the reduction potential when the water partial pressure is increased resulting in a particle morphology with a lower surface area.

Similarly, it has been reported that the reaction order of CO is positive (38, 44). From a microscopic point of view this is also difficult to understand since methanol is synthesized from CO_2 (26, 27). However, a positive reaction order can be explained within the present dynamic model since higher concentrations of CO increase the reduction potential of the synthesis gas resulting in a more flat particle with a larger surface area.

3. CONCLUSIONS

A detailed microkinetic analysis of the methanol synthesis reaction has been presented. Based on the changes in particle morphology observed previously by EXAFS, a dynamic microkinetic model has been developed. This model is able to describe the change in particle morphology (i.e., the number of active sites and the exposed facets) with change in gaseous environment as well as the reaction rate over the three basal Cu surface planes. It is found that it is crucial to include this description in order to describe kinetic data measured at industrial relevant conditions over a Cu/ZnO catalyst. The picture that emerges reveal that metallic copper is the active phase in methanol synthesis but the interaction between copper and zinc oxide is important for the dynamic spreading of the copper particles on the support. Due to the structure sensitive nature of the reaction the morphology changes have very pronounced effects on the catalytic activity. It is furthermore seen that these dynamical changes have consequences for interpretation of the observed reaction orders.

ACKNOWLEDGMENTS

We thank I. Chorkendorff, J. B. Hansen, P. E. Højlund Nielsen, and E. Törnqvist for valuable discussions. This work was supported by the Danish Research Councils through the Center for Surface Reactivity and through the Center for Atomic-scale Material Physics.

REFERENCES

1. Froment, G. F., and Bischoff, K. B., "Chemical Reactor Analysis and Design." Wiley, New York, 1979.
2. Boudart, M., and Djéga-Mariadassou, G., "Kinetics of Heterogeneous Catalytic Reactions." Princeton Univ. Press, Princeton, NJ, 1984.
3. Dumesic, J. A., Rudd, D. F., Aparicio, L. M., Rekoske, J. E., and Treviño, A. A., "The Microkinetics of Heterogeneous Catalysis." Am. Chem. Soc. Washington, DC, 1993.
4. Stoltze, P., and Nørskov, J. K., *Phys. Rev. Lett.* **55**, 2502 (1985); Stoltze, P., and Nørskov, J. K., *J. Catal.* **110**, 1 (1988).
5. Oh, S. H., Fisher, G. B., Carpenter, J. E., and Goodman, D. W., *J. Catal.* **100**, 360 (1986).
6. Hellsing, B., Kasemo, B., Ljungström, S., Rosén, A., and Wahnström, T., *Surf. Sci.* **189/190**, 851 (1987).
7. Hickman, D. A., and Schmidt, L. D., *AIChE J.* **39**, 1164 (1993).
8. Hinrichsen, O., Rosowski, F., Muhler, M., and Ertl, G., *Chem. Eng. Sci.* **51**, 1683 (1996).
9. Bartholomew, C. H., and Boudart, M., *J. Catal.* **29**, 278 (1973).
10. Williams, F. L., and Boudart, M., *J. Catal.* **30**, 438 (1973).
11. Nielsen, J. R., "Steam Reforming Catalysts." Teknisk Forlag, Copenhagen, 1975.
12. Leyrer, J., Zaki, M. I., and Knözinger, H., *J. Phys. Chem.* **90**, 4775 (1986).
13. Knözinger, H., *in* "Proceedings, 9th International Congress on Catalysis, Calgary, 1968" (M. J. Phillips and M. Ternan, Eds.). Chem. Institute of Canada, Ottawa, 1988.
14. Knözinger, H., and Taglauer, E., *Catalysis* **10**, 1 (1993).
15. Somorjai, G. A., "Introduction to Surface Chemistry and Catalysis." Wiley, New York, 1994.
16. Derouane, E. G., Baker, R. T. K., Dumesic, J. A., and Sherwood, R. D., *J. Catal.* **69**, 101 (1981).
17. Dumesic, J. A., Topsøe, H., and Boudart, M., *J. Catal.* **37**, 513 (1975).
18. Clausen, B. S., Steffensen, G., Fabius, B., Villadsen, J., Feidenhans'l, R., and Topsøe, H., *J. Catal.* **132**, 524 (1991).
19. Clausen, B. S., Schiøtz, J., Gråbæk, L., Ovesen, C. V., Jacobsen, K. W., Nørskov, J. K., and Topsøe, H., *Topics Catal.* **1**, 367 (1994).
20. Clausen, B. S., Gråbæk, L., Steffensen, G., Hansen, P. L., and Topsøe, H., *Catal. Lett.* **20**, 23 (1993).

21. Nielsen, J. R., and Højlund Nielsen, P. E., *in* "Deactivation and Poisoning of Catalysts" (J. Oudar and H. Wise, Eds.). Dekker, New York, 1985.
22. Wulff, G., Z. Krastallog. **34**, 449 (1901).
23. Brands, D. S., Poels, E. K., Krieger, T. A., Makarova, O. V., Weber, C., Veer S., and Bliek, A., *Catal. Lett.* **36**, 175 (1996).
24. Askgaard, T. S., Nørskov, J. K., Ovesen, C. V., and Stoltze, P., *J. Catal.* **156**, 229 (1995).
25. Muhler, M., Törnqvist, E., Nielsen, L. P., Clausen, B. S., and Topsøe, H., *Catal. Lett.* **25**, 1 (1994).
26. Rozovskii, A. Ya., *Kinet. Katal.* **21**, 97 (1980).
27. Chinchen, G. C., Denny, P. J., Parker, D. G., Spencer, M. S., and Whan, D. A., *Appl. Catal.* **30**, 333 (1987).
28. Ovesen, C. V., Stoltze, P., Nørskov, J. K., and Campbell, C. T., *J. Catal.* **134**, 445 (1992).
29. Ovesen, C. V., Clausen, B. S., Hammershøi, B. S., Steffensen, G., Askgaard, T., Chorkendorff, I., Nørskov, J. K., Rasmussen, P. B., Stoltze, P., and Taylor, P., *J. Catal.* **158**, 170 (1996).
30. Rasmussen, P. B., Holmblad, P. M., Askgaard, T. S., Ovesen, C. V., Stoltze, P., Nørskov, J. K., and Chorkendorff, I., *Catal. Lett.* **26**, 373 (1994).
31. Fujitani, T., Nakamura, I., Watanabe, T., Uchijima, T., and Nakamura, J., *Catal. Lett.* **35**, 297 (1995).
32. Yoshihara, J., and Campbell, C. T., *J. Catal.* **161**, 776, (1996).
33. Stull, D. R., and Prophet, H. (Eds.), "JANAF Thermochemical Tables," 2nd ed., Nat. Bur. of Standards, Washington, DC, 1971.
34. Chorkendorff, I., Physics Department, Technical University of Denmark, unpublished results.
35. Harendt, C., Goschnick, J., and Hirchwald, W., *Surf. Sci.* **152/153**, 453 (1985).
36. Taylor, P. A., Rasmussen, P. B., Ovesen, C. V., Stoltze, P., and Chorkendorff, I., *Surf. Sci.* **261**, 191 (1992).
37. Ying, D. H. S., and Madix, R. J., *J. Catal.* **61**, 48 (1980).
38. Graaf, G. H., Stamhuis, E. J., and Beenackers, A. A. C. M., *Chem. Eng. Sci.* **43**, 3185 (1988).
39. Graaf, G. H., Ph.D. thesis, Rijksuniversiteit Groningen, 1988.
40. Ludviksson, A., Zhang, R., Campbell, C. T., and Griffiths, K., *Surf. Sci.* **313**, 64 (1994).
41. Topsøe, N.-Y., Haldor Topsøe Research Laboratories, Denmark, manuscript in preparation.
42. Dybkjær, I., Højlund Nielsen, P. E., and Hansen, J. B., paper presented at the 73rd Annual Meeting AIChe, New Orleans, 1980.
43. Liu, G., Willcox, D., Garland, M., and Kung, H. H., *J. Catal.* **90**, 139 (1984).
44. Chinchen, G. C., Denny, P. J., Jennings, J. R., Spencer, M. S., and Waugh, K. C., *Appl. Catal.* **36**, 1 (1988).
45. Vanden Bussche, K. M., and Froment, G. F., *J. Catal.* **161**, 1 (1996).